MCNP6 and Serpent 2 results comparison in the neutronic modelling of aqueous homogeneous subcritical systems for medical isotope production

Liván Hernández Pardo*

Instituto Superior de Tecnologías y Ciencias Aplicadas (InSTEC),
Universidad de La Habana,
La Habana, Cuba
Email: lhernandez@instec.cu
*Corresponding author

Daylen Milian Pérez

Departamento de Energía Renovable y Eficiencia Energética,
Cubaenergía,
Playa, La Habana, Cuba
Email: dmperez@cubaenergia.cu

Daniel Milian Pérez

Departamento de Energia Nuclear,
Universidade Federal de Pernambuco (UFPE),
Recife, Pernambuco, Brazil
Email: daniel.milian@ufpe.br

Daniel E. Milian Lorenzo

Instituto Superior de Tecnologías y Ciencias Aplicadas (InSTEC),
Universidad de La Habana,
La Habana, Cuba
Email: dmilian@instec.cu

Carlos A. Brayner de Oliveira Lira

Centro Regional de Ciências Nucleares (CRCN-NE/CNEN),
Cidade Universitária,
Recife, Pernambuco, Brazil
Email: brayner@cnen.gov.br

Abstract: In this paper, a computational model using Monte Carlo codes has been implemented for the modelling of an accelerator-driven Aqueous Homogeneous Subcritical Systems (AHSS) conceptual design for medical isotope production. It aims to contribute to the verification and validation of the computational model and the most up-to-date evaluated nuclear data libraries for the AHSS study. The calculation tasks performed were to compute and

compare the AHSS neutronic parameters of interest using two widely used codes, MCNP6 and Serpent 2. The results section is divided into three main types of calculation: criticality calculations, fixed-source calculations and fuel depletion/burnup calculations. All percentage differences between the results of the codes are generally lower than 1% and agree within the statistical precision of the codes with a confidence level of 99.7%.

Keywords: AHSS; aqueous homogeneous subcritical systems; MCNP6; Serpent 2; ENDF/B; JEFF; medical isotopes.

Reference to this paper should be made as follows: Pardo, L.H., Pérez, D.M., Pérez, D.M., Lorenzo, D.E.M. and de Oliveira Lira, C.A.B. (2021) 'MCNP6 and Serpent 2 results comparison in the neutronic modelling of aqueous homogeneous subcritical systems for medical isotope production', *Int. J. Nuclear Energy Science and Technology*, Vol. 15, No. 1, pp.61–78.

Biographical notes: Liván Hernández Pardo is Professor at the Instituto Superior de Tecnologías y Ciencias Aplicadas (InSTEC), Cuba. He graduated in Engineering in Nuclear and Energy Technologies from the InSTEC in 2020. His research interests include nuclear engineering with emphasis on physics, thermohydraulic and mechanical design, modelling, simulation and analysis of advanced nuclear systems.

Daylen Milian Pérez Graduated in Engineering in Nuclear and Energy Technologies from the Instituto Superior de Tecnologías y Ciencias Aplicadas (InSTEC) in 2020. His research interests include nuclear engineering with emphasis on physics, thermohydraulic and mechanical design, modelling, simulation and analysis of advanced nuclear systems.

Daniel Milian Pérez Graduated in Engineering in Nuclear and Energy Technologies from the Instituto Superior de Tecnologías y Ciencias Aplicadas (InSTEC) in 2013. He completed his Master's degree in Energy and Nuclear Installations from InSTEC in 2015, PhD degree in Energetic and Nuclear Technologies from the Department of Nuclear Energy (DEN) at the Federal University of Pernambuco (UFPE) in 2020. His research interests include nuclear engineering with emphasis on physics, neutronic, thermohydraulic and mechanical design, modelling, simulation and analysis of advanced nuclear systems.

Daniel E. Milian Lorenzo is Professor at the Instituto Superior de Tecnologías y Ciencias Aplicadas (InSTEC), Cuba. He received his PhD degree in Nuclear Engineering in 2001 and BSc degree in Nuclear Engineering in 1980 at the Higher Institute Jose Antonio Echeverria (CUJAE). He has researched in nuclear reactors physics since more than 35 years. He has published more than 30 papers in international journals.

Carlos A. Brayner de Oliveira Lira holds his degree in Electronic Engineering from the University of Pernambuco in 1976, a Master's degree in Energy and Nuclear Technologies from the Federal University of Pernambuco in 1980 and a Doctorate in Nuclear Engineering – Universitat Hannover in 1984. He was a Professor at the Federal University of Pernambuco from 1979 to 2019. His research interests include nuclear engineering with an emphasis on reactor technology and nuclear instrumentation, acting mainly on the following topics: reactor thermohydraulic, perturbative methods, sensitivity analysis and innovative reactors. Currently, he is Director of the Regional Centre for Nuclear Sciences of the Northeast CRCN/NE.

1 Introduction

Special attention has been paid to Aqueous Homogeneous Reactors (AHR) for medical isotope production, in particular molybdenum-99 (^{99}Mo). Lower capital cost and potentially lower operating costs, higher safety standards, easier processing and handling of irradiated fuel, less generation of nuclear waste and more efficient neutron utilisation than heterogeneous research reactors are the main advantages of AHRs for this application (IAEA, 2008). Recently, some governments and private entities have carried out a new approach based on AHRs and particle accelerators, the accelerator-driven Aqueous Homogeneous Subcritical System (AHSS) (National Academies of Sciences Engineering and Medicine, 2018; Syarip et al., 2018). This technology enhances the strengths and reduces the weakness of AHR and accelerators for the production of medical isotopes (Piefer et al., 2011). Several neutronic and thermal-hydraulic studies have been accomplished by researchers using computational simulation for the conceptual design and evaluation of AHSS (Gholamzadeh et al., 2015; Mirvakili et al., 2016; Kim and Buechler, 2017; Syarip et al., 2018; Yassar et al., 2018; Nazarudin et al., 2020; Kim et al., 2020; Hernández et al., 2021; Ren et al., 2021).

Accurate modelling of these systems is of substantial importance in understanding their multi-physics behaviour in all possible situations and operation regimes. This fact has become more possible with improvements in computer hardware, the development of advanced computational codes and the generation of more accurate nuclear data libraries. Verification and validation of such codes and data libraries should be performed for each application to be studied by comparing the calculation results with experimental measurements. Typically, for nuclear reactor applications, neutronic calculation codes are validated by contrasting the calculation results with criticality benchmarks such as those listed in the International Criticality Safety Benchmark Evaluation Project (ICSBEP) (Nuclear Energy Agency, 2020), as well as comparing them with the plant operational data.

In the case of AHSS, currently under development, the experimental measurements published for the scientific community is limited, as this is a novel technology. Even for AHRs, the available information about experiments is scarce. In cases like this, researchers often make code-to-code comparisons and use different nuclear data sources to verify the agreement between the calculation results with distinct tools (Kromar and Kurinčič, 2013; Alferov et al., 2015; Dumen et al., 2017; Edwards et al., 2020).

In this paper, the two Monte Carlo codes MCNP6 (Armstrong et al., 2017) and Serpent 2 (Leppänen, 2015) have been implemented in the modelling of an AHSS conceptual design for medical isotope production. It aims to contribute to the verification and validation of the computational model and the most up-to-date evaluated nuclear data libraries for the AHSS study. The calculation tasks were oriented to compute and compare the most interesting neutronic parameters of the AHSS, for this, the results section was divided into three main types of calculation: criticality calculations, fixed-source calculations and fuel depletion/burnup calculations. In the criticality calculations, the temperature dependence of the effective multiplication factor (k_{eff}) was determined with both codes, this is a very important characteristic in the coupled neutronic thermal-hydraulic calculation for the multi-physics study of fission chain-reacting systems. In addition, a subcritical state was estimated using the latest releases of two evaluated

nuclear data libraries, the ENDF/B and the JEFF files, at room temperature. The fixed-source type of calculation was used to estimate the neutron energy spectrum and the volumetric distribution of the fission energy deposited in the fuel solution. Finally, the depletion/burnup calculation was employed to evaluate the production of the medical isotopes ^{99}mo, iodine-131 (^{131}I), Xenon-133 (^{133}Xe) and strontium-89 (^{89}Sr).

2 Materials and methods

2.1 AHSS conceptual design description

The AHSS conceptual design analysed in this paper was detailed in Hernández et al. (2021). The AHSS conceptual design is a modified version of the Russian ARGUS reactor (Glouchkov and Khvostionov, 1997; Pérez et al., 2015, 2017, 2019, 2020, 2021) configured for operating in a subcritical state and assisted by a Deuterium-Tritium (D-T) neutron generator. The subcritical system showed in Figure 1 is made up of a cylindrical stainless-steel vessel with a hemispherical bottom 0.5 cm thick and 30.5 cm internal diameter, containing an aqueous solution of uranyl sulphate (UO_2SO_4). The vessel has a height of 71.5 cm and is surrounded by a graphite reflector in the shape of a rectangular parallelepiped. A vertical channel of a 7.95 cm diameter tube penetrates by the centre of the vessel from above, this is intended for the tritium gas target. Inside the vessel and immersed in the aqueous solution, there are three helical cylindrical pipes into which flows water as a cooling fluid, the objective of this pipe system is to maintain the temperature of the homogeneous mixture below 90ºC. Table 1 resumes the main parameters and properties of the UO_2SO_4 aqueous solution at 20ºC.

Table 1 Main parameters of the uranyl sulphate aqueous solution at 20ºC

Parameter	*Value*	*Unit*
Enrichment in ^{235}U	19.8	%
Concentration	390	g-U/L
Density	1.5073	g/cm^3
Volume	28759	cm^3
Surface height	52.4	cm

A neutron generator with a tritium gas target based on a linear accelerator of low energy deuterons was used as a neutron source. The D-T fusion reaction has a high cross-section for the formation of helium-4 (^{4}He) and neutrons with 14.1 MeV, with a peak of 5 barn around 109 keV (Richardson, 2019). For this conceptual design, a 300 keV deuteron beam energy was assumed to impact a 2.4 kPa Tritium gas target. The graph of Figure 2 shows the beam energy dissipation as well as the normalised neutron production yield per unit of length and current along the gas target. This feature is very important for the neutron source modelling, it was determined assuming a theoretical methodology employed in Hernández et al. (2021) and proposed by (Piefer, 2014).

Figure 1 Schematic view of the AHSS conceptual design

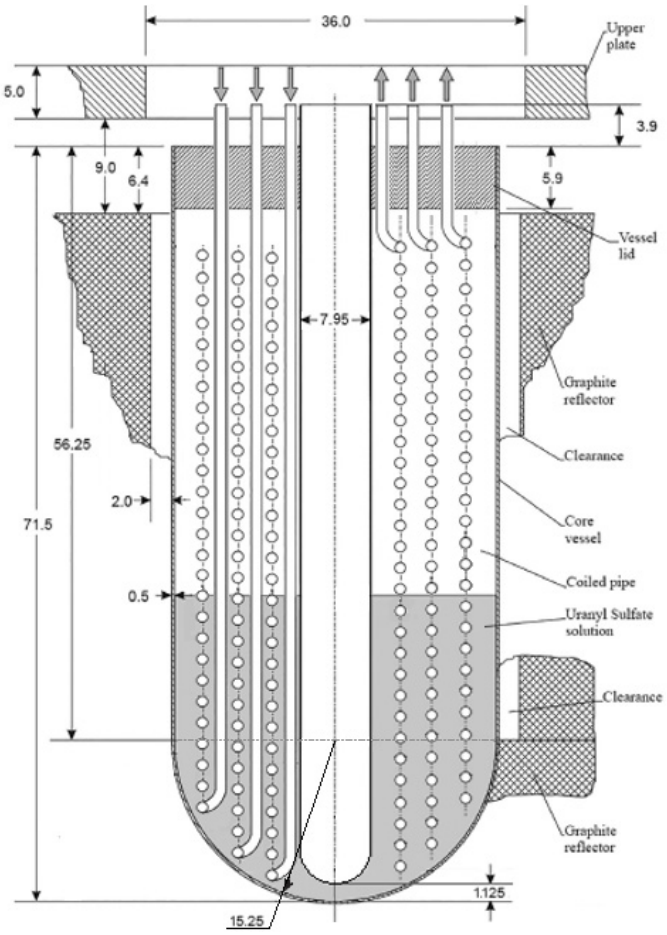

Figure 2 Beam energy and normalised neutron yield per current and length unit along the gas target

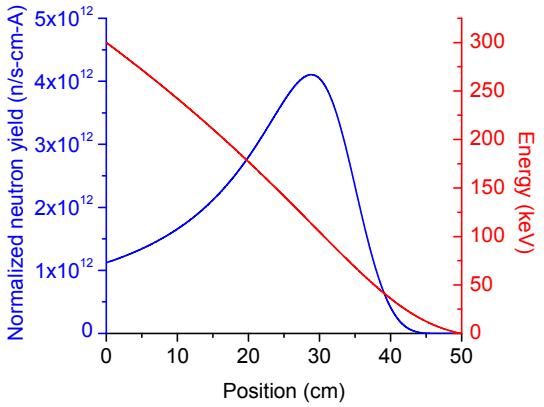

2.2 Neutronic models and codes description

The Monte Carlo N-Particle (MCNP) particle transport code is a general-purpose three-dimensional simulation tool that calculates the transport of 37 different types of particles in criticality, dosimetry, effect on detectors and other applications. It can be used in different modes of transport: neutron, photon or electron only, neutron/photon combined transport where photons are produced by interactions of neutrons, neutron/photon/electron, photon/electron, or electron/photon. This includes the ability to calculate eigenvalues for critical systems, to calculate the particle transport in fixed-source mode, and to perform the burnup/depletion and transmutation of materials. The code version used was the MCNP6 v1.0, which was released in 2013 (Armstrong et al., 2017).

Similar to MCNP, Serpent (Leppänen, 2015) is a multi-purpose three-dimensional continuous-energy Monte Carlo particle transport code. This was developed at VTT Technical Research Centre of Finland and it has been publicly distributed by the OECD/NEA Data Bank and RSICC since 2009. Serpent started as a simplified reactor physics code, but the capabilities of the current development version, Serpent 2, extend well beyond reactor modelling. Although this code was initially created with the idea to be a well-suited code for lattice physics applications, especially group constant generation, Serpent has been extended for multiple applications. They are divided into three categories: 1) traditional reactor physics applications, including spatial homogenisation, criticality calculations, fuel cycle studies, research reactor modelling, validation of deterministic transport codes and others; 2) multi-physics simulations, i.e. coupled calculations with thermal-hydraulics, CFD and fuel performance codes and 3) neutron and photon transport simulations for radiation dose rate calculations, shielding, fusion research and medical physics (Serpent, 2021). In this work, the Serpent 2.1.29 specific version was used.

2.2.1 MCNP6 and Serpent 2 models

The AHSS conceptual design model developed in Hernández et al. (2021) with MCNP6 was used here. A longitudinal section view of the full 3D geometrical model of the AHSS is shown in Figure 3. The helical pipes represented by equally spaced toroids (2 cm) were the only simplification that was made to the geometrical model since they cannot be modelled exactly in MCNP6. The neutron source was modelled as a 1 cm^2 cross-section cylinder concentric to the vertical channel (see Figure 3); from which neutrons are born isotropically at 14.1 MeV. The normalised neutron yield per current and length unit (see Figure 2) was used to define a discretised probability distribution for the neutron source along the vertical direction. This distribution was discretised with 31 points and MCNP6 uses linear interpolation for points between them (see Figure 4).

In this paper, the AHSS conceptual design was also modelled in Serpent 2. An identical full 3D geometry to MCNP6 was generated, including the coiled pipes simplification (see Figure 3) (Serpent 2 can accomplish the real coiled pipes model). The neutron source modelling was performed in a similar way to MCNP6, but the probability distribution was discretised in sections with a constant value equal to the mean between the extreme values of each interval (see Figure 4).

Figure 3 View of a longitudinal section of the geometrical model in a) MCNP6 and b) Serpent 2

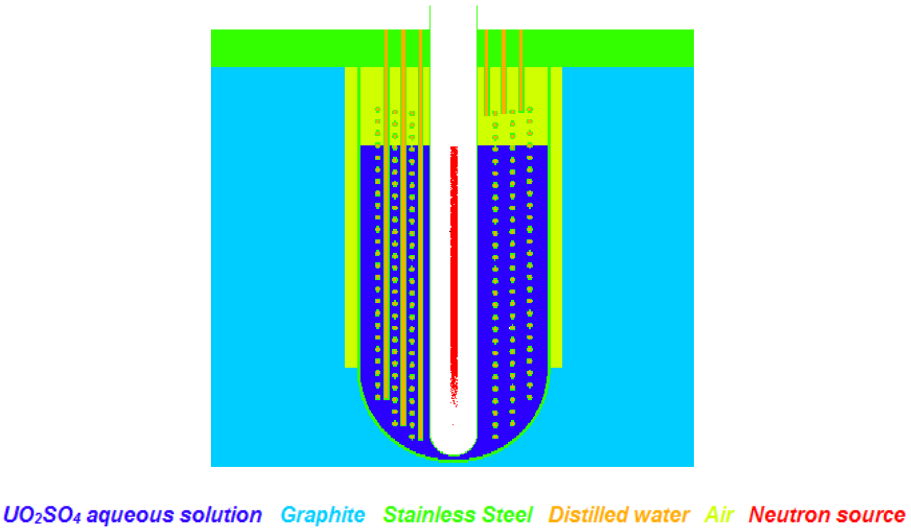

Figure 4 Discretisation of the neutron source probability distribution in MCNP6 and Serpent 2

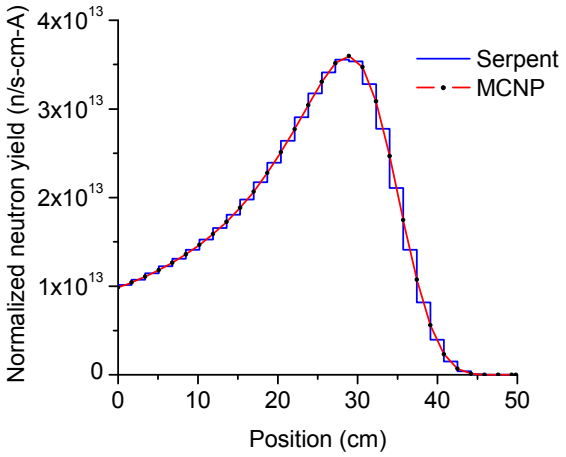

2.2.2 Nuclear data libraries

In contribution with the verification and validation process for nuclear data to transport codes, evaluated nuclear data libraries from two different sources were used. The VII.0, VII.1 and VIII.0 releases of the evaluated ENDF/B library were utilised in the MCNP6 and Serpent 2 calculations. In addition, the JEFF-3.1, JEFF-3.2 and JEFF-3.3 libraries were employed. These libraries contain the continuous-energy neutron interaction data and the neutron $S(\alpha,\beta)$ thermal data necessary for the proper neutron transport in such codes. MCNP6 and Serpent 2 read those evaluated data in the ACE (A Compact ENDF) format, which are elaborated with the nuclear data processing code NJOY (Macfarlane

et al., 2017) and distributed with the codes. The ENDF/B-VIII.0-based ACE library was acquired from the Los Alamos National Laboratory (LANL) distribution site for nuclear data libraries (Los Alamos National Security, 2018), and the ACE libraries based on the JEFF-3.2 and JEFF-3.3 were obtained from the OECD/NEA (Nuclear Energy Agency of the Organisation for Economic Co-operation and Development) Data Bank web site (NEA Nuclear Data Services, 2018; OECD/NEA, 2021). The other libraries are distributed with the codes.

Table 2 shows the available ACE libraries for all isotope/elements involved in the AHSS models. Also the neutron $S(\alpha,\beta)$ thermal data libraries are specified for hydrogen in light water (H-H_2O), graphite and hydrogen in polyethylene (H-CH_2). All used libraries are evaluated at 293.6 K, except for the JEFF-3.1 library, which is at 300 K. In the case that an ACE library does not exist for a particular isotope/element, this was supplied with the library indicated in Table 2. The JEFF-3.3-based ACE library uses the new continuous representation of the $S(\alpha,\beta)$ thermal data, which is not compatible with the Serpent 2.1.29 version, that is why the JEFF-3.2-based ACE library was used in this case.

Table 2 Nuclear data libraries used for each isotope or element in all materials

Isotope/element	*ENDF/B*			*JEFF*		
ZAID	*VII.0*	*VII.1*	*VIII.0*	*3.1*	*3.2*	*3.3*
1001	✓	✓	✓	✓	✓	✓
5010	✓	✓	✓	✓	✓	✓
5011	✓	✓	✓	✓	✓	✓
6012	ENDF/ B-V.0	ENDF/ B-V.0	✓	ENDF/ B-V.0	ENDF/ B-V.0	ENDF/ B-V.0
7014	✓	✓	✓	✓	✓	✓
8016	✓	✓	✓	✓	✓	✓
14028	✓	✓	✓	✓	✓	✓
15031	✓	✓	✓	✓	✓	✓
16032	✓	✓	✓	✓	✓	✓
18000	LANL/T	LANL/T	LANL/T	LANL/T	LANL/T	LANL/T
22000	ENDF/ B-VI.8	ENDF/ B-VI.8	ENDF/ B-VI.8	ENDF/ B-VI.8	ENDF/B-VI.8	ENDF/ B-VI.8
24052	✓	✓	✓	✓	✓	✓
25055	✓	✓	✓	✓	✓	✓
26056	✓	✓	✓	✓	✓	✓
29063	✓	✓	✓	✓	✓	✓
92234	✓	✓	✓	✓	✓	✓
92235	✓	✓	✓	✓	✓	✓
92236	✓	✓	✓	✓	✓	✓
23238	✓	✓	✓	✓	✓	✓
H-H_2O	✓	✓	✓	✓	✓	✓
Graphite	✓	✓	✓	✓	✓	✓
H-CH_2	✓	✓	✓	JEFF-3.2	✓	JEFF-3.2

2.3 Methodology

All the calculations carried out in this work were divided into three sections, classifying them by type of calculation: criticality calculations, fixed-source calculations, and fuel depletion/burnup calculations.

2.3.1 Criticality calculations

The interconnected nature between thermal-hydraulic and neutron transport phenomena makes the multi-physics study of nuclear reactors and subcritical systems necessary for the correct understanding of their behaviour in different accident scenarios or operating conditions. To accomplish this study, neutron transport and thermal-hydraulic codes are coupled in an iterative calculation process. One of the most important aspects of such analysis is the good representation of the temperature changes in the system for the neutronic calculations.

In this section, two calculations tasks were carried out. The first one consisted of calculating the k_{eff} of the AHSS conceptual design for several subcritical states varying the uniform temperature of the aqueous solution in each one. Supposing that the normal operating temperature range of the AHSS is 20 to 90ºC, as assumed in Hernández et al. (2021), eight configurations from 20 to 90ºC with steps of 10ºC were calculated.

To simulate the temperature effect over the system reactivity, two main aspects were taken into account: the thermal expansion of the aqueous solution and the variation of the neutron interaction cross-sections. The thermal expansion was included by modifying the mass density of the aqueous solution, but the increase of the solution volume was not modelled considering this is negligible. For MCNP6, the cross-section libraries for each temperature were created using the MCNP utility program makxsf (Brown, 2006). This program incorporates routines from the NJOY (Macfarlane et al., 2017) and DOPPLER (MacFarlane and Talou, 2003) codes to provide for Doppler broadening of resolved data to any higher temperature, and for interpolating $S(\alpha,\beta)$ thermal scattering kernels and probability tables for unresolved resonance data between two bracketing temperatures (Brown, 2006). Serpent 2 uses its built-in Doppler-broadening pre-processor routine for adjusting the temperatures of ACE format cross-sections; also, it interpolates between tabular data for adjustment of neutron thermal scattering cross-section and energy-angle distributions in $S(\alpha,\beta)$ format (Serpent, 2021).

The second calculation task involved the re-calculation of the 20ºC subcritical state of the AHSS conceptual design with both codes using the six different evaluated ENDF/B and JEFF libraries.

All the eigenvalue problems were calculated using 50 and 1000 inactive and active cycles respectively, with 15,000 histories per cycle in both codes. The Serpent 2 code uses two approaches to calculate the k_{eff}-eigenvalue, the analogue and the implicit estimator (Leppänen, 2015), both of which were considered for the comparisons in this work.

2.3.2 Fixed-source calculations

Fixed-source calculations were performed to calculate important features that depend on the external neutron source. The first task was to determine the neutron energy spectrum

in the aqueous solution volume. For this, the energy range of 0.001 eV to 15 MeV was considered and this interval was divided into 200 lethargy-normalised bins.

The second topic consisted in computing the spatial distribution of the fission energy deposited in the solution volume. For this, a cylindrical tally mesh was superimposed over the aqueous solution volume composed of 130 points in the radial direction and 500 points in the vertical direction. Only one bin was established in the angular direction considering that the system geometry has axial symmetry.

These two calculation types were performed using the ENDF/B-VII.1 library at 293.6 K. The neutron source was modelled as explained in Sub-section 2.2.1 for each code and 4 million histories were recorded.

2.3.4 Depletion/burnup calculations

By last, the medical isotope production was quantitatively estimated by the depletion/ burnup calculation. The calculations with both codes were executed considering a nominal thermal power of 20 kW_{th} in ten operation days. The calculation time step for both codes was chosen as one day. In each time step, a predictor-corrector approach is applied by the codes using 1000 active and 50 inactive cycles, respectively. In order to reduce the computational requirements, 5000 histories per cycle was set. For MCNP6, the CINDER decay and fission yield data library was used, which is based on the ENDF/B-VI.0 evaluation. While for Serpent 2, this data type was adopted from the ENDF/B-VI.8 data source. The accumulation of mass and activities of ^{99}Mo, ^{89}Sr, ^{133}Xe and ^{131}I were recorded.

3 Results and discussion

Calculation results were reported in the same order as explained above.

3.1 Criticality calculations

The first results of the subcriticality calculations are shown in Table 3. This reports the k_{eff} eigenvalues calculated with MCNP6 and Serpent 2 and their respective standard deviations for eight different subcriticality states. In the case of Serpent 2, the analogue (A_k_{eff}) and implicit (I_k_{eff}) estimates of k_{eff} are specified. The last two columns contain the percentage differences between the two Serpent 2 estimates and MCNP6 calculated as:

$$\frac{k_{MCNP6} - k_{Serpent}}{\left(k_{MCNP6} + k_{Serpent}\right)/2} \times 100\% \tag{1}$$

It can be seen that all percentage differences are smaller than 0.1% and only for the 70ºC case it is higher than 0.05% with the Serpent 2 implicit approach.

Additionally, these calculations results were graphically illustrated in Figure 5, where a 3σ error bar graph is used for their comparison. It shows the good agreement of the two codes results for the different temperature states, which demonstrates the good temperature treatment of the codes. Note that each k_{eff} value for all temperature states is within the 3σ size interval (a confidence level of 99.7%) of the others.

Table 3 Eigenvalues calculated with MCNP6 and Serpent 2 for the eight temperature states

Temp (ºC)	*MCNP6*	*Serpent 2*		*Differences %*	
	k_{eff} (±0.00020)	A_k_{eff} (±0.00033)	I_k_{eff} (±0.00024)	*A_Diff*	*I_Diff*
20	0.98744	0.98733	0.98746	0.011	–0.002
30	0.98417	0.98440	0.98396	–0.024	0.022
40	0.98045	0.98055	0.98047	–0.011	–0.002
50	0.97725	0.97727	0.97711	–0.002	0.014
60	0.97316	0.97321	0.97336	–0.005	–0.020
70	0.96998	0.96958	0.96939	0.041	0.061
80	0.96646	0.96641	0.96613	0.005	0.034
90	0.96254	0.96261	0.96266	–0.007	–0.012

Figure 5 Comparison of eigenvalues calculated by MCNP6 and Serpent 2 for the eight temperature states (3σ error bars)

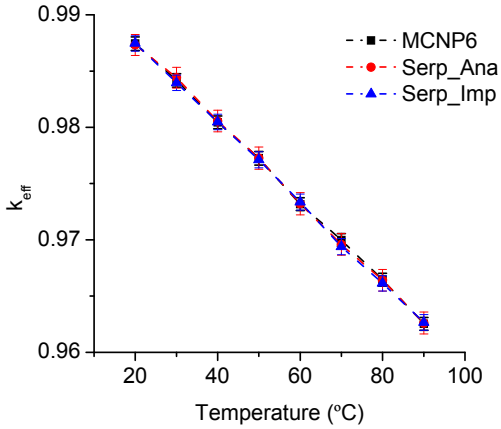

On the other hand, Table 4 shows the calculation results regarding the verification of several data libraries sources. This contains the k_{eff} eigenvalues calculated with MCNP6 and Serpent 2 using three ENDF/B and three JEFF libraries at 20ºC. Also, the percentage differences were reported resulting in absolute values less than 0.5%, only the ENDF/B-VIII.0 case was higher than 0.1%. For each code, the standard deviation of the six-group results was calculated and specified at the end of each column, this evidence a bigger dispersion in the Serpent 2 results.

From another point of view, Figure 6(a) presents the graphical analysis of the previous results. This graph compares the k_{eff} values calculated with each library for the two codes. In the case of MCNP6, the results are less dispersed than the Serpent 2 results, which is related to the standard deviation of the two codes results. This trend suggests that the MCNP6 solver is more precise for the same histories account recorded. As can be noted, the results with the ENDF/B libraries are always higher than those with the JEFF libraries. Figure 6(b) demonstrates the good agreement between the codes calculation results for all libraries.

Table 4 Eigenvalues calculated with MCNP6 and Serpent 2 with different data libraries sources

Library	*MCNP6*	*Serpent 2*		*Differences %*	
	k_{eff} *(±0.00020)*	*A_*k_{eff} *(±0.00033)*	*I_*k_{eff} *(±0.00023)*	*A_Diff*	*I_Diff*
endf70	0.98698	0.987504	0.987282	–0.053	–0.031
endf71	0.98744	0.987327	0.987460	0.011	–0.002
endf80	0.98767	0.988798	0.988699	–0.114	–0.104
jeff31	0.98582	0.985295	0.985393	0.053	0.043
jeff32	0.98555	0.985330	0.985315	0.022	0.024
jeff33	0.98601	0.986580	0.986289	–0.058	–0.028
σ	0.0009	0.0014	0.0013	–	–

Figure 6 Comparison between a) data libraries sources (3σ error bars) and between b) MCNP6 and Serpent 2 (3σ error bars)

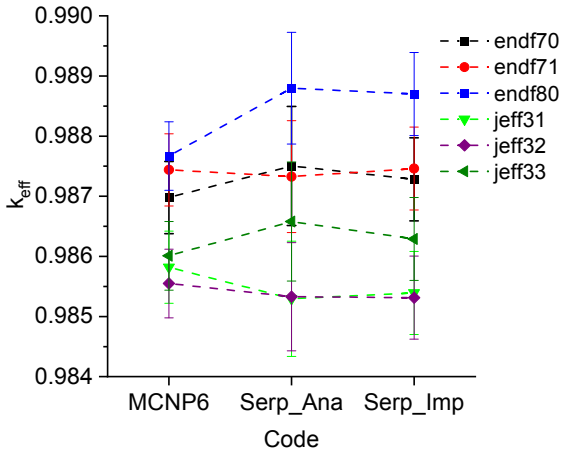

(a)

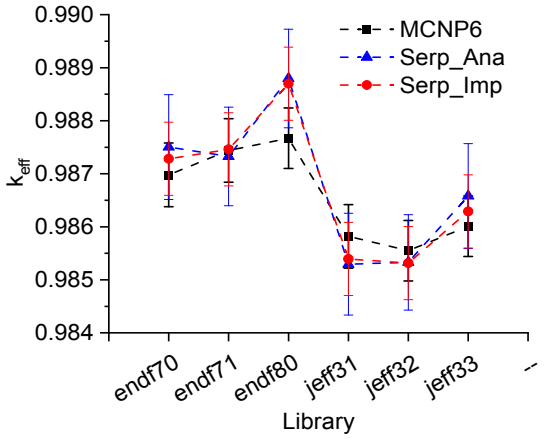

(b)

3.2 Fixed-source calculations

In this section, the results regarding the fixed-source calculation type were reported. First, the energy neutron spectrum was determined by the two codes. Figure 7 shows the normalised neutron flux (per neutron source intensity n/s) in the energy range divided by lethargy-normalised 200 bins. The two peaks evidence the thermal behaviour of the subcritical system. Above the 10 MeV energy, it can be noted a third lowest peak due to the contribution of the 14.1 MeV neutron source. The percentage differences between the neutron spectrums calculated by the two codes (see Figure 7) reach 0.96% and the MCNP6 results generally exceed the Serpent 2 ones by 0.79%.

Figure 7 Energy neutron spectrums (with 3σ error bars) in the aqueous solution calculated by the codes and their percentage differences

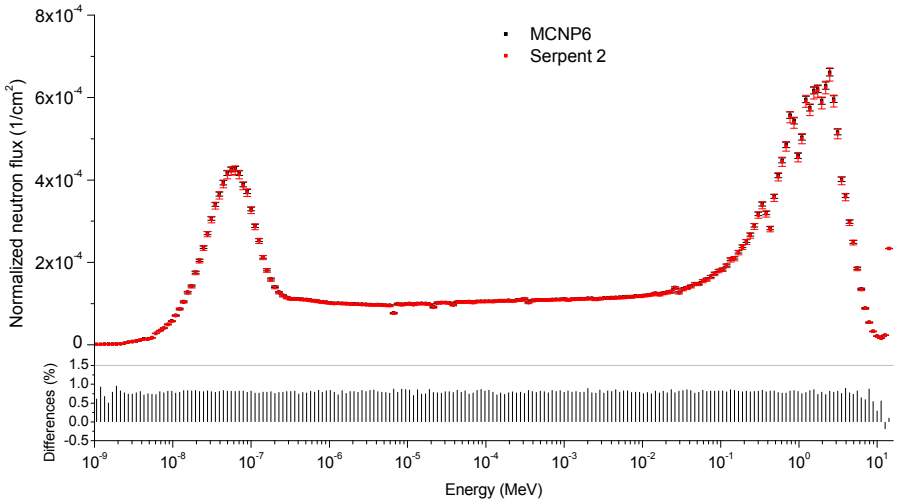

Figures 8(a) and 8(b) show the spatial distribution of the fission energy density δP normalised to the average value of fission energy density δP_{ave} deposited in the aqueous solution volume determined by the codes MCNP6 and Serpent 2, respectively. It is appreciable a peak close to half of the solution height and to the central channel, which is in part influenced by the higher neutron source intensity in this zone. With a simple view of these graphs, it is possible to appreciate the similarity in the two profiles, Figure 8(c) exposes the percentage differences that are below 5%. The differences are almost uniformly distributed over the solution. Figure 9 shows that more than 85% of all mesh points of the two normalised fission energy density profiles agree with less than 1%, while the differences are less than 2% for more than 98% of the points. Mesh points with differences larger than 5% only represent 0.3%, these points are located in the lowest zone of the aqueous solution, just below the central channel. It is supposed that this zone is much less populated with neutrons than the rest of the solution, consequently, Monte Carlo codes record fewer fission events and this makes the tally less precise and less trustworthy.

Figure 8 Spatial distribution of the normalised fission energy density deposited in the solution calculated by a) MCNP6, b) Serpent 2 and c) Absolute values of the percentage differences

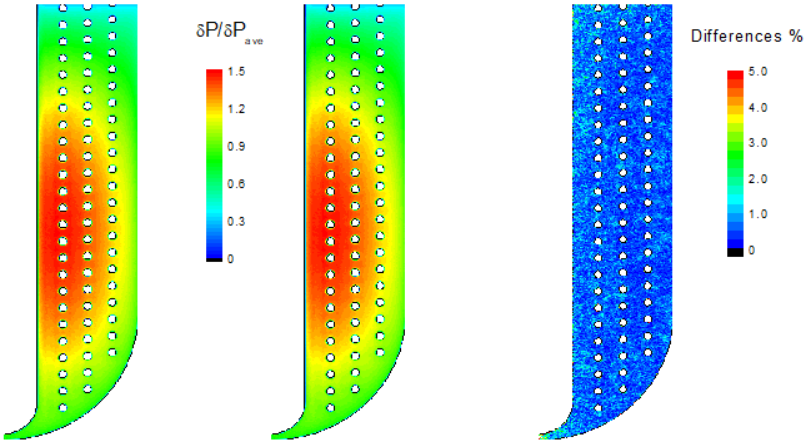

Figure 9 Percentage frequencies distribution and percentage cumulative frequencies of the percentage differences between the fission energy density profiles

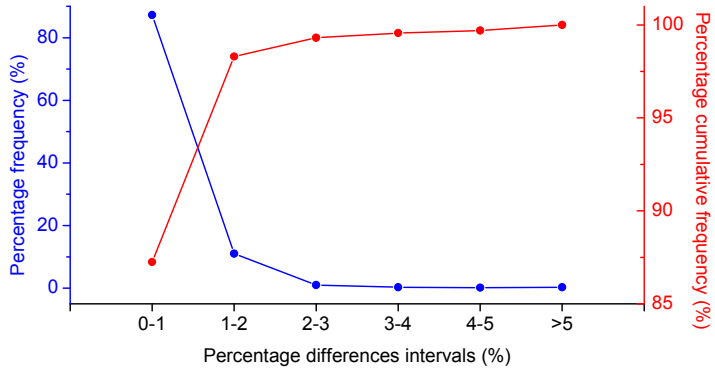

3.3 Depletion/burnup calculations

In ten days of the aqueous solution irradiation at 20 kW_{th} of thermal power, the fuel solution burnup reaches only 17.83 MWd/MTU. It was verified that the variation in k_{eff} is lower than their standard deviation.

The last task was accomplished by calculating the buildup of the isotopes of interest. Figures 10a, 10c, 10e and 10g show the accumulated mass of ^{99}Mo, ^{89}Sr, ^{131}I and ^{133}Xe, respectively, in ten days of continuous irradiation calculated with MCNP6 and Serpent 2. Figures 10(b), 10(d), 10(f) and 10(h) exhibit the percentage differences between the two code estimations. As it can appreciate, the percentage differences are less than 1% in all cases, except for the ^{131}I isotope, which reaches a value of 3%. In the case of ^{99}Mo, the differences do not follow a clear trend, therefore, they may be associated only with the statistical precision of both codes.

On the other hand, the percentage differences between the codes estimates for the ^{89}Sr, ^{131}I and ^{133}Xe nuclides tend to increase with time and the Serpent 2 estimations of nuclides mass are always larger than the MCNP6 ones. This may be a consequence of not using the same decay and fission yields libraries. However, it is expected that the main reason for those discrepancies is correlated to the different isotope generation algorithms of both codes. While Serpent 2 automatically activates a wide range of nuclides generated during the transmutation calculations, MCNP6 tracks only certain decay chains, which may obviate important isotopes like ^{89}Se, ^{89}Br, ^{89}Kr, ^{89}Rb, ^{131}Te, ^{131m}Te, ^{133}I and ^{133m}Xe that leads to the production of ^{89}Sr, ^{131}I and ^{133}Xe by beta decay reactions. Nevertheless, the percentage differences increase with a tendency to stabilise for a time greater than ten days.

Figure 10 Accumulation of a) ^{99}Mo, c) ^{89}Sr, e) ^{131}I and f) ^{133}Xe masses in ten days calculated with both codes and their respective percentage differences b), d), f) and h)

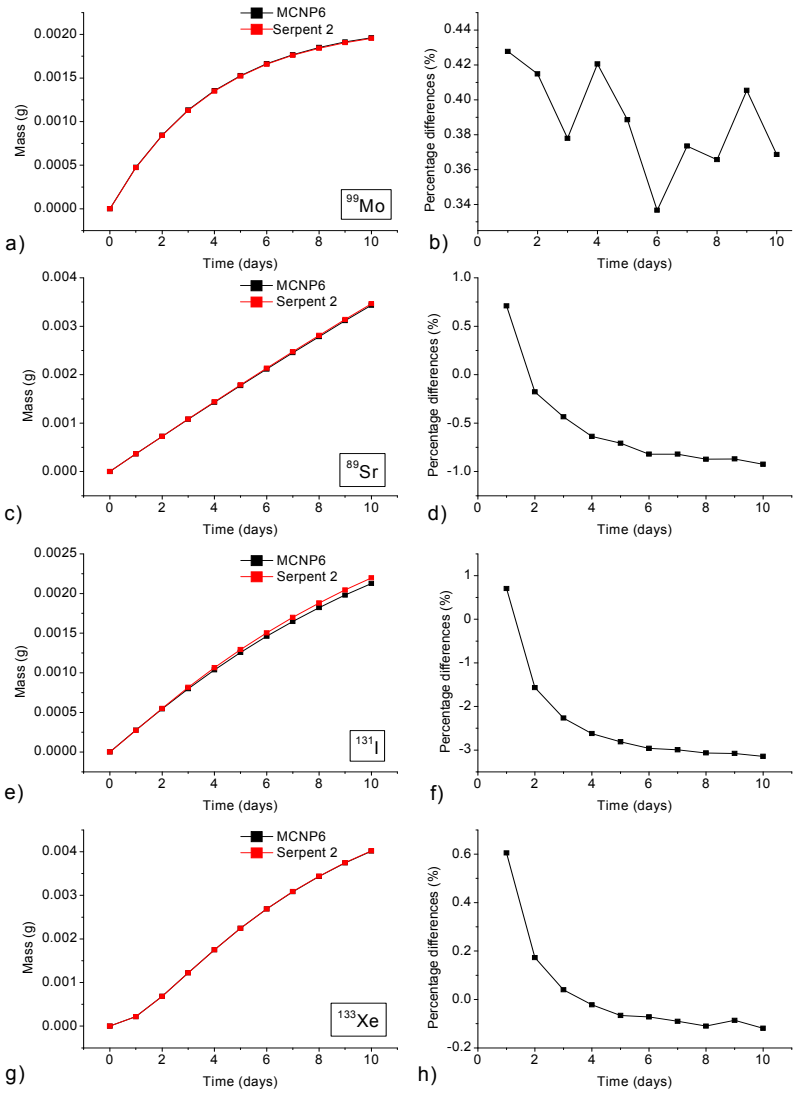

4 Conclusions

In this paper, the two Monte Carlo codes MCNP6 and Serpent 2 have been implemented in the modelling of an AHSS conceptual design for the partial verification and validation of the computational model developed and the most up-to-date evaluated nuclear data libraries. The calculations were orientated to compute and compare the most interesting neutronic parameters of the AHSS, for this, three main types of calculation were carried out: criticality calculations, fixed-source calculations, and fuel depletion/burnup calculations.

In the criticality calculations, the temperature dependence of the effective multiplication factor was determined with both codes, resulting in that all percentage differences between the k_{eff} estimates were smaller than 0.1% and were within the statistical precision of each value. The k_{eff} eigenvalues calculated with MCNP6 and Serpent 2 using three ENDF/B and three JEFF libraries at 20ºC result in percentage differences less than 0.5%, only the ENDF/B-VIII.0 case was higher than 0.1%. The k_{eff} estimations with Serpent 2 using all libraries were more dispersed about a central value than the MCNP6 ones. The results with the ENDF/B libraries were always higher than those with the JEFF libraries for both codes.

Regarding the fixed-source type of calculation, the percentage differences between the neutron energy spectrums calculated by the two codes reach 0.96% and the MCNP6 results generally exceed the Serpent 2 ones by 0.79%. However, the normalised neutron flux values by the two codes agree with a confidence level of 99.7%. The volumetric distribution of the fission energy deposited in the fuel solution results in that more than 85% of all mesh points agree with less than 1% between the codes, while the differences are less than 2% for more than 98% of the points.

Finally, the depletion/burnup calculation was employed to evaluate the production of the medical isotopes ^{99}Mo, ^{131}I, ^{133}Xe and ^{89}Sr. The percentage differences were less than 1% in all cases, except for the ^{131}I isotope, which can reach a value of 3%. However, the percentage differences increase with a tendency to stabilise for a time greater than ten days.

Finally, the two codes and six nuclear data libraries used showed good agreement between them. Thus, the computational model developed for the AHSS study can be suitably implemented applying these tools.

Acknowledgement

This research was partially supported by the Coordenação de Aperfeiçoamento de Pessoal de Nível Superior (CAPES), project no: 88887.518186/2020-00.

References

Alferov, V.P. et al. (2015) 'Comparative validation of Monte Carlo codes for the conversion of a research reactor', *Annals of Nuclear Energy*, Vol. 77, pp.273–280. Doi: 10.1016/j.anucene.2014.11.032.

Armstrong, J. et al. (2017) *MCNP® User's Manual Code Version 6.2*, *LA-UR-17-29981*, Christopher, J.W. (Ed.), Los Alamos National Laboratory (LANL).

Brown, F.B. (2006) *The makxsf Code with Doppler Broadening*, *LA-UR-06-7002*, Los Alamos National Laboratory (LANL).

Dumen, V.M., Ternovykh, M.Y. and Abu Sondo, M.A. (2017) 'The verification of the complex programs serpent 2 and scale (SAS2) for analysing the safety characteristics of FA reactor vver-1000 at all the operation stages', *Proceedings of the 13th International Youth Scientific and Practical Conference 'Future of Atomic Energy*, pp.201–218. Doi: 10.18502/keg.v3i3.1620.

Edwards, G.W.R., Colton, A.V. and Bromley, B.P. (2020) 'Differences in exit burnup, depletion, and fuel reactivity calculations arising from the choice of modelling code for bundles with thorium and uranium', *CNL Nuclear Review*, Vol. 9, No. 1, pp.57–71. Doi: 10.12943/CNR.2018.00011.

Gholamzadeh, Z. et al. (2015) 'Computational investigation of ^{99}Mo, ^{89}Sr, AND ^{131}I production rates in a subcritical $UO_2(NO_3)_2$ Aqueous solution reactor driven by a 30-mev proton accelerator', *Nuclear Engineering and Technology*, Vol. 47, No. 7, pp.875–883. Doi: 10.1016/j.net.2015.08.004.

Glouchkov, E.S. and Khvostionov, V.E. (1997) *Graphite-Reflected Uranyl Sulphate (20.9% ^{235}U) Solutions*, *NEA/NSC/DOC/(95)03/III, IEU-SOL-THERM-001*, Russian Research Center "Kurchatov Institute".

Hernández, L. et al. (2021) 'Coupled multi-physics simulation for the evaluation of an accelerator-driven aqueous homogeneous subcritical system for medical isotope production', *Progress in Nuclear Energy*, Vol. 134. Doi: 10.1016/j.pnucene.2021.103692.

IAEA (2008) *Homogeneous Aqueous Solution Nuclear Reactors for the Production of Mo-99 and other Short Lived Radioistotopes*, *IAEA-TecDoc-1601*, Vienna. Available online at: https://n9.cl/scb6q

Kim, S.J. and Buechler, C.E. (2017) *Development of Multi-physics (Multiphase CFD + MCNP) Simulation for Generic Solution Vessel Power Calculation*, *LA-UR-17-25931*, Los Alamos National Laboratory (LANL). Doi: 10.2172/1371685.

Kim, S.J., Verner, K.M. and Larsen, A.W. (2020) *Design Optimization of A generic Fissile Solution for Mo99 Production using Electron Beam-based Neutron Generator using MCNP+CFD*, *LA-UR-20-23069*. Los Alamos National Laboratory (LANL).

Kromar, M. and Kurinčič, B. (2013) 'Comparison of the SCALE, SERPENT and MCNP criticality safety calculation of the NPP Krško Spent Fuel Pool', *Journal of Energy*, Vol. 62, pp.200–208. Available online at: https://hrcak.srce.hr/199060.

Leppänen, J. (2015) *Serpent – a Continuous-energy Monte Carlo Reactor Physics Burnup Calculation Code*, VTT Technical Research Centre of Finland.

Los Alamos National Security (2018) *Nuclear Data Libraries from Los Alamos National Laboratory*, *nucleardata.lanl.gov*. Available online at: https://nucleardata.lanl.gov/ACE/Production/Lib80x.html (accessed on 12 May 2021).

Macfarlane, R. et al. (2017) *The NJOY Nuclear Data Processing System, Version 2016*, *LA-UR-17-20093*, Los Alamos National Laboratory (LANL). Available online at: https://www.osti.gov/servlets/purl/1338791

MacFarlane, R.E. and Talou, P. (2003) *DOPPLER: A Utility Code for Preparing Customized Temperature-Dependent Data Libraries for the MCNP Monte Carlo Transport Code*, Los Alamos National Laboratory (LANL).

Mirvakili, S.M., Gholamzadeh, Z. and Davari, A. (2016) 'Neutronic and thermo hydraulic analysis of a modeled subcritical uranyl nitrate aqueous reactor driven by 30-MeV protons', *Annals of Nuclear Energy*, Vol. 97, pp.171–178. Doi: 10.1016/j.anucene.2016.06.037.

National Academies of Sciences Engineering and Medicine (2018) *Opportunities and Approaches for Supplying Molybdenum-99 and Associated Medical Isotopes to Global Markets: Proceedings of a Symposium*, The National Academies Press, Washington, DC. Doi: 10.17226/24909.

Nazarudin, M.A. et al. (2020) 'Safety analysis of gas pressure in a subcritical assembly for molybdenum-99 production system', *Journal of Southwest Jiaotong University*, Vol. 55, No. 3. Doi: 10.35741/issn.0258-2724.55.3.49.

NEA Nuclear Data Services (2018) *JEFF-3.3*. Available online at: https://www.oecd-nea.org/dbdata/jeff/jeff33/index.html (accessed on 15 May 2021).

Nuclear Energy Agency (2020) *ICSBEP Handbook 2020*, Nuclear Energy Agency. Doi: 10.1787/7e0ebc50-en.

OECD/NEA (2021) *JEFF-3.2 Evaluated Data Library - Neutron Data*. Available online at: https://www.oecd-nea.org/dbforms/data/eva/evatapes/jeff_32/ (accessed on 18 May 2021).

Pérez, D.M. et al. (2015) 'Thermal-hydraulics study of a 75 kWth aqueous homogeneous reactor for ^{99}Mo production', *Journal of Thermodynamics*, pp.1–11. Doi: 10.1155/2015/268034.

Pérez, D.M. et al. (2017) 'Effects of some calculation parameters on the computational modelling of temperature, velocity and gas volume fraction during steady-state operation of an aqueous homogeneous reactor', *International Journal of Nuclear Energy Science and Technology*, Vol. 11, No. 1, pp.1–21. Doi: 10.1504/ijnest.2017.10005993.

Pérez, D.M. et al. (2019) 'Neutronic evaluation of the steady-state operation of a 20 kWth aqueous homogeneous reactor for Mo-99 production', *Annals of Nuclear Energy*, Vol. 128, pp.148–159. Doi: 10.1016/j.anucene.2019.01.002.

Pérez, D.M. et al. (2020) 'New advances in the computational simulation of Aqueous Homogeneous Reactor for medical isotopes production', *Brazilian Journal of Radiation Sciences*, Vol. 8, No. 3A, pp.1–18. Doi: 10.15392/bjrs.v8i3A.1409.

Pérez, D.M. et al. (2021) 'Multi-physics evaluation of the steady-state operation of an aqueous homogeneous reactor for producing Mo-99 for the Brazilian demand', *International Journal of Thermodynamics*, Vol. 24, No. 1, pp.9–22. Doi:10.5541/ijot.790728.

Piefer, G. (2014) *High Energy Proton or Neutron Source*, USA. Available online at: https://n9.cl/s9fa

Piefer, G. et al. (2011) *Mo-99 Production Using a Subcritical Assembly*, Mo-99 Topical Meeting, Santa Fe, New Mexico. Available online at: https://n9.cl/sd8u

Ren, L. et al. (2021) 'Neutronics study of a subcritical system driven by external neutron source for 99Mo production', *Fusion Engineering and Design*, Vol. 165. Doi: 10.1016/j.fusengdes.2021.112263.

Richardson, A.S. (2019) *2019 NRL PLASMA FORMULARY*, *NRL/PU/6770--19-652*. Available online at: https://www.nrl.navy.mil/ppd/content/nrl-plasma-formulary

Serpent (2021) *Serpent – a Continuous-energy Monte Carlo Reactor Physics Burnup Calculation Code*. Available online at: http://montecarlo.vtt.fi/ (accessed on 18 June 2021).

Syarip, A. et al. (2018) 'Design and development of subcritical reactor by using aqueous fuel for ^{99}Mo production', *Proceedings of the Pakistan Academy of Sciences: A. Physical and Computational Sciences*, pp.21–26.

Yassar, F., Harto, A.W. and Syarip, A. (2018) 'Neutronic analysis of subcritical assembly for ^{99}Mo isotope production based on thorium nitrate fuel', *Proceedings of the 3rd Padjadjaran International Physics Symposium*. Doi: 10.1088/1742-6596/1080/1/012021.